Numerical & Experimental Study to Evaluate the Performance of Universiti Tenaga Nasional Short Duration Hypersonic Test Facility

Al-Falahi Amir[1], Yusoff M. Z[2], & Yusaf T[3]

[1]Universiti Industri Selangor "UNISEL", Faculty of Engineering, Jalan Timur Tambahan, 45600 Batang Berjuntai, Selangor Darul Ehsan, Malaysia

[2]University Tenaga Nasional "UNITEN", College of Engineering, Jalan Puchong-Kajang, 43009 Kajang, Selangor Darul Ehsan, Malaysia

[3]University of Southern Queensland "USQ", Faculty of Engineering and Surveying, Toowoomba 4350, Australia

E-mail: alfalahi@unisel.edu.my

Abstract

The work of this paper is aimed to investigate the parameters that affect the performance of a short-duration hypersonic test facility that build at the Universiti Tenaga Nasional "UNITEN" in Malaysia. The facility has been designed, constructed, and commissioned for different values of diaphragm pressure ratios and different gas combinations. The applications and reasoning behind building such a facility are explained. The governing equations for the shock wave are presented. A theoretical model was developed to evaluate the shock wave strength P_2/P_1 values as a function of diaphragm pressure ratio P_4/P_1 for different driver/driven gas combinations. A two-dimensional time-accurate time-marching Navier-Stokes solver for shock wave applications is described. It uses second-order accurate cell-vertex finite-volume spatial discretization and fourth order accurate Runge-Kutta temporal integration. Experimental tests for different operating conditions have been accomplished. A high precision pressure transducer and an in house made thermocouple were used to measure the pressure history which represents the shock wave strength P_2/P_1 and the surface temperature change profile during the facility operation. A MATLAB numerical transient heat transfer model was developed to evaluate the heat flux from the surface temperature change history. The calculated parameters which are pressure, temperature and shock wave velocity, and the CFD results were found to be much matched comparable to the experimental results.
.

Introduction Historically, a large number of methods have been used to improve the performance of high speed flow test facilities (e.g. shock tubes, gun tunnels, and shock tunnels) [1]. One of these methods is to fill the driver section with a light gas such as helium while the driven section is to be filled with heavy gas such as CO_2 or N_2. Another is to increase the temperature of the driver gas by use of a heater. In both of these methods, the improved performance is achieved by a higher speed of sound than if cold air is used. In the first case, the speed of sound in helium is higher than air because of its lower molecular weight. In the latter, the speed of sound is increased by raising the gas temperature. When higher sound speed is used, a lower driver-to-driven tube pressure ratio P_4/P_1 is required to generate a given incident shock Mach number in the driven tube.

Physical Description of UNITEN's Facility

The detail components of the facility are described briefly and shown in Figure 1 (for further details and operating procedure see ref. [2]). The facility consists of the following significant items as can be seen in Figure 1.
1. Driver section: a high-pressure section (driver), which will contain the high pressure driver gas.

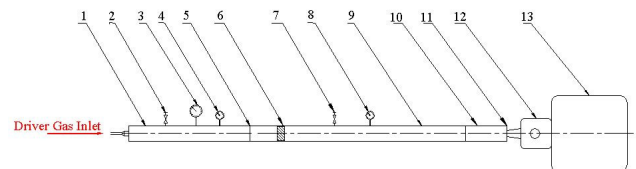2. Discharge valve: to discharge the driver section after each run.

Figure 1: A schematic diagram of UNITEN's 'HTF'

3. Pressure gauge: to read the pressure inside the driver section, this section is also provided with a static pressure transducer to record the exact value of the driver pressure P_4 at which the diaphragm ruptures.
4. Vacuum pump: when the driver gas is not air (e.g. Helium or Hydrogen) then the driver section should be evacuated and refilled with the required driver gas.
5. The primary diaphragm: this is a thin aluminum membrane to isolate the low-pressure test gas from the high-pressure driver gas until the compression process is initiated.
6. Piston compression section: A piston is placed in the barrel (driven tube) adjacent to the primary diaphragm so that when the diaphragm ruptures, the piston is propelled through the driven tube, compressing the gas ahead of it. This piston used with gun tunnel tests only.
7. Discharge valve: to discharge the driven section after each run.
8. Vacuum gauge: to set the pressure inside the barrel section to low values (vacuum values) less than atmospheric value.
9. Barrel section: a shock tube section (smooth bore), to be filled with the required test gas (air, nitrogen or carbon dioxide).
10. Barrel extension: the last half meter of the barrel on which the pressure transducers and thermocouples are to be attached (see details in Fig.4).
11. The secondary diaphragm: it is a light plastic diaphragm to separate the low pressure test gas inside the barrel from the test section and dump tank which are initially at a vacuum prior to the run.
12. Test section: this section will expands the high temperature test gas through a nozzle to the correct high enthalpy conditions needed to simulate hypersonic flow. A range of Mach numbers is available by changing the diameter of the throat insert.
13. Vacuum vessel (dump tank): to be evacuated to about 0.1 mm Hg pressure before running. Prior to a run, the barrel, test section, and dump tank are to be evacuated to a low-pressure value.

Reasoning Behind Building This Facility

Construction of this facility is fundamentally important for the development of advanced instrumentation (in this case, fiber optic pressure sensors and fast response thermocouples), and heat transfer/fluid mechanics studies that are relevant to turbine and

aerodynamics investigations. It can provide a convenient and low cost experimental facility that can produce the necessary flow conditions (matched Mach and Reynolds numbers, temperature ratios etc) for any specific experimental simulation environment.

This facility can be used in wide range of important applications such as:
1. High temperature gases in physics and chemistry,
2. Testing of supersonic bodies and hypersonic entry vehicles,
3. Developing of high power gas dynamic and chemical lasers,
4. It is a basic tool in understanding of high-speed compressible flow,
5. An important application of unsteady wave motion,
6. Interactions between two shocks,
7. Studies of the physics of instabilities induced by shocks passing through fluid boundaries of different density,
8. Developing of specialized instrumentation for measuring the physical properties of shocked gases, and
9. Validation of computer codes.

Formulation of the CFD Code
Mathematical Model
The governing fluid flow equations are presented in concert with the numerical scheme used to compute the compressible flow within the shock tube.

Reynolds-Averaged Navier-Stokes Equations (RANS)
The two-dimensional continuity, x- and y-momentum and energy equations describing the turbulent flow of a compressible fluid expressed in strong conservation form in the x-, y-Cartesian co-ordinate system may be written as

$$\frac{\partial \underline{w}}{\partial t} + \frac{\partial \underline{F}}{\partial x} + \frac{\partial \underline{G}}{\partial y} = \underline{J}$$

(1)

where $\underline{w}$ represents the conserved variables and $\underline{F}$ and $\underline{G}$ are the overall fluxes in x-, y-directions respectively.

The Mixing Length Turbulence Model
In the current work, the Prandtl's mixing length model is considered:

$$\mu_t = \rho l_m^2 \left|\frac{\partial u}{\partial y}\right|$$

(2)

where l_m is the mixing length and $\frac{\partial u}{\partial y}$ is the velocity gradient (using Gauss Divergence Theorem). Here, the main flow direction is assumed to be in the x-direction.

Rodi (1980) has suggested several algebraic expressions to predict the mixing length. The following mixing length formulation, which is designed for pipes (geometrical similarity with shock tube), is used.

$$l_m = L[0.14 - 0.08(1 - y/L)^2 - 0.06(1 - y/L)^4]$$

(12)

Here, L is the radius of the shock tube (= 0.025m) and y is the nearest distance from the bounded walls. The values of the nearest distance are pre-computed before the solution stage. More recent details about the mixing length formulations can be found in Veersteg and Malalasekera (1995).

Solution Algorithm
Starting from the flow field variables obtained from the previous time step, the conserved variables in RANS are solved with the appropriate boundary conditions (see Section Boundary Conditions), using the multi-stage Runge-Kutta scheme explained later. Within the iterative loop of the Runge-Kutta

scheme, the second-order Jameson type scheme is used for space discretisation. The updated variables are then computed at the end of each time step. The process is iterated until the desired time level is reached.

Cell-Vertex Finite-Volume Spatial Discretization
The flow domain is replaced by a finite number of grid points, which are generated algebraically by the current solver. The mesh system is commonly known as H-mesh and divides the physical domain into a set of discrete rectangular control volumes. An example of H-mesh is shown in Figure 2.
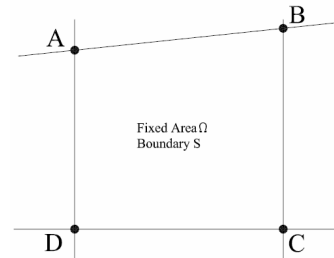

Figure 2:   An illustration of a typical 2D H-mesh.

A cell-vertex formulation is used in which the flow variables are stored at cell vertices A, B, C and D as has been shown in Figure 2. Cell-vertex formulation offers some advantages over the cell-centered one in which cell-vertex method offers higher accuracy on irregular grid. For a uniform mesh, there would be no difference between the cell-centered and cell-vertex schemes; however, cell-vertex scheme does not require extrapolation to the solid boundary to obtain the wall static pressure, which is necessary in solving the momentum equations for cells adjacent to the solid boundary.

Starting from known values of primitive variables from the previous time-step, the values of F and G are determined at each node. Then the line integration is performed for each control volume in turn for the four conserved variables.
The discretized RANS:

$$R_{ij} =$$
$$-\frac{1}{\Omega_{ij}} \oint (F_{ijC}dy - G_{ijC}dx) + \frac{1}{\Omega_{ij}} \oint (F_{ijV}dy - G_{ijV}dx)$$
$$+ \frac{1}{\Omega_{ij}} \oint (F_{ijT}dy - G_{ijT}dx) + J$$

(3)

After the spatial integration, Equation (1) will take the form: -

$$\left(\frac{\partial \underline{w}}{\partial t}\right)_{ij} = R_{ij}(\underline{w})$$

(4)

in which $R_{ij}(\underline{w})$ represents the residual for each cell.

The calculated residuals apply to the values of properties within the cell, whereas, the variables are actually stored at the nodes. Consequently, they have to be redistributed to the four surrounding nodes. This is done by sharing the changes equally between the four nodes as shown in Figure 5.2, as suggested in the second-order central differencing scheme. Thus:

$$R_A(\underline{w}) = 0.25(R_{i,j-1} + R_{i,j} + R_{i-1,j-1} + R_{i-1,j})$$

(5)

For nodes at the wall, since two cells share a single node, the residual obtained from Equation (3) is doubled.

Thus, the equivalent discretized equation for node A will be:

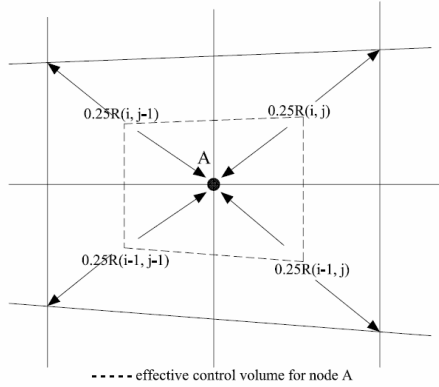$$\left(\frac{\partial w}{\partial t}\right)_A = R_A(\underline{w})$$

(6)

Figure 3: Distribution of cell residual to nodes.

Boundary Conditions
Solid Boundary
Only the solid boundary condition is considered in the current work since the flow is confined within the tube. At the wall, no-slip boundary condition is imposed for the momentum equations to enforce no mass fluxes can penetrate through the solid boundary. For the energy equation, adiabatic condition is assumed.

Initial Conditions
To start the iterations, initial flow field variables must be specified at all calculating points. In the current work, the pressure values are specified at both the driver and driven sections, in accordance with the desired pressure ratio. Initially, gas assumed to be stationary in all sections of the facility.

Solution Flowchart
Step 1: Generate the structured H-mesh. The details of the mesh system will be explained later.
Step 2: Initialise the flow variables at time = 0s.
Step 3: Initiate the 4-stage Runge-Kutta (RK) time integration scheme. Here, the artificial viscosity and the laminar/turbulent shear stresses are calculated for the first RK stage, followed by the spatial integration of the governing equations to determine the residual in Equation 3. The cell residuals are then redistributed back to the neighbouring vertices using Equation 5. The solution vector is then time marched using the residuals for each vertex and the corresponding stage coefficient (α).The flow variables are then updated accordingly.
Step 4: Step 3 is repeated until the maximum Runge-Kutta stage (in this case is 4) is reached.
Step 5: Save the pressure value at the first station (refer to Figure 6). Update the time level ($t^{n+1}=t^n+\Delta t$). Go to Step 3 until the desired time level is reached.

CFD Code Validation
The computer program was checked by running simulations for several simple gasdynamic systems. Simulations of the interaction of a shock wave with an abrupt area change indicated that the two-dimensional formulation used here could reliably capture shocks and the effect of area changes. Viscous effects were checked by simulating the flow in a low-pressure shock tube, the correct shock speed was computed for the low-pressure

shock tube, the speed of the contact surfaces was well approximated.

Results and discussion
Three sets of runs were performed to evaluate the facility performance. In the first group of runs air has been used as a driver/driven gas. The second group of tests used the Helium/Air as driver/driven gases, and the last group of experiments used the Helium/CO_2 driver/driven gases. Two pressure transducers and surface junction thermocouple have been mounted in the barrel extension (item 10 in Fig. 1) with an axial separation of 342 mm as shown in Figure 4.
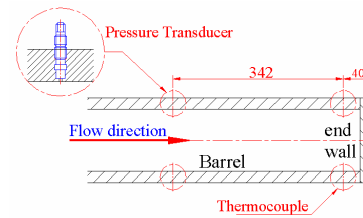

Figure 4: Pressure transducers and thermocouple

The in-cylinder pressure was measured by a commercial quartz pressure transducer (PCB mode number 111A24) and an inline charge amplifier (PCB model number 402A03) was used. The facility has been modified to give closed end shock tube arrangement.

CFD Simulation Setting
A FORTRAN program has been developed, mainly to generate the required input data for the flow solver. The input data includes, for instances, the time step size (Δt) for the Runge-Kutta time integration method, the number of time-step (NMAX), the driver pressure (P_4), the driven pressure (P_1), the maximum cell spacing in both the x- (JM) and y-(IM) direction, the flow model (inviscid/viscous) as well as the fluid properties. In the current work, the author has simulated the shot (air-air) on a fixed mesh system: JMxIM =355x31.
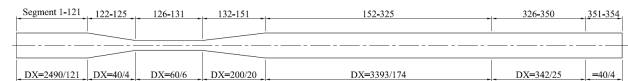

Figure 5: Mesh spacing allocated for each section

As shown in Figure 5, the author has included an artificial wedge simply to represent the bush located adjacent to the primary diaphragm to facilitate the rupture process. This is due to the nature of the code used, whereby it is not able to handle abrupt change in geometry effectively. A variety of wedge angles has been simulated and the angle of 7° yields the best agreement against the experimental result.

Numerical Simulation and Experimentation for Similar Gases (air-air)
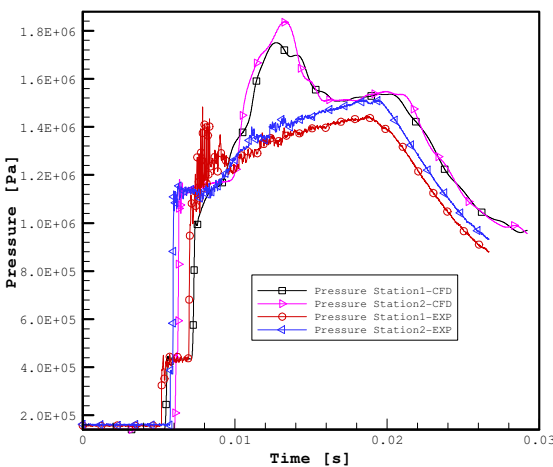Figure 6 compares the CFD result with respect to those measured at three different pressure ratios for the air-air case. As seen, the agreement of the pressure values predicted at both the first and second stations is very promising. At higher pressure ratio, the shock wave strength will be augmented as predicted from both sets of solutions.
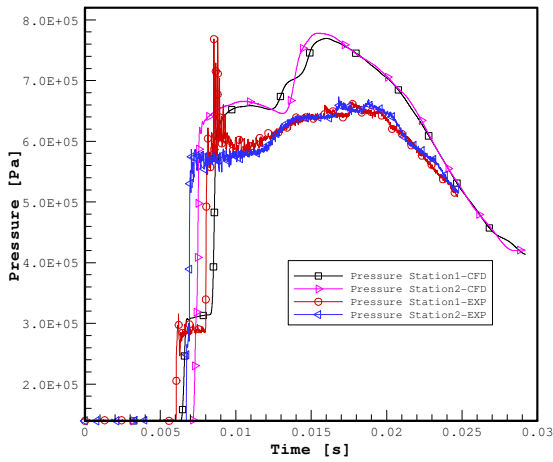
(a) $P_4/P_1=8.4$
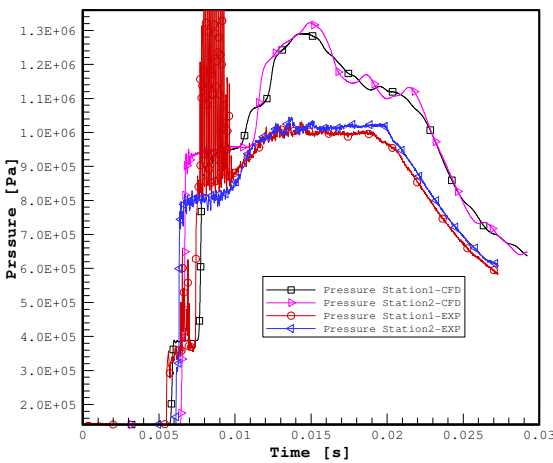
(b) $P_4/P_1=15$

(c) $P_4/P_1=20$

Figure 6: Experimental & CFD Pressure history inside the barrel at different pressure ratios (air-air).

In order to examine closely the shock strength, a close up view of the incident shock wave and reflected shock wave has been

generated as shown in Figure 7. Interestingly enough, the error level between the numerical and the experimental result is only marginal. The predicted shock wave strength using CFD is always higher compared to that of experimental work, which may be due to the discretisation error inherited in the convective differencing schemes, the mesh/time resolution error, the assumption of adiabatic wall boundary condition, etc. Also, from the experimental work it has been shown that there is deposition of chips at the right end of the barrel. This indicates that the chip is traveling along with the shock wave during the run time and this has not been taken into account in the numerical model.
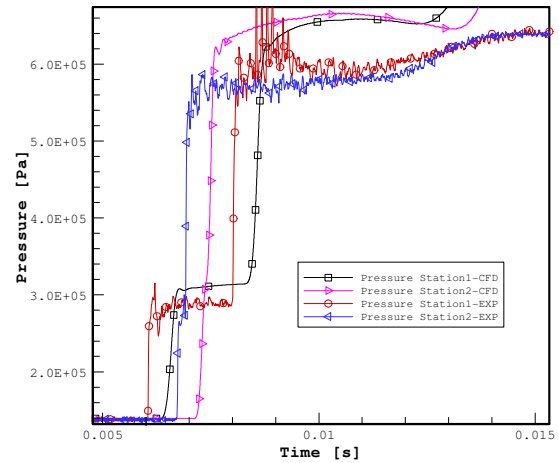
Figure 7: Shock wave speed and shock wave strength at $P_4/P_1=8.4$.

To summaries the observations of shock speed, shock strength as well as the pressure peak value, Figure 8 has shown the pressure plots at 3 different pressure ratios obtained from both the CFD and experimental data. As observed, the shock speed is increased when the pressure ratio is augmented. This condition holds true even for the shock strength as well as the pressure peak value.
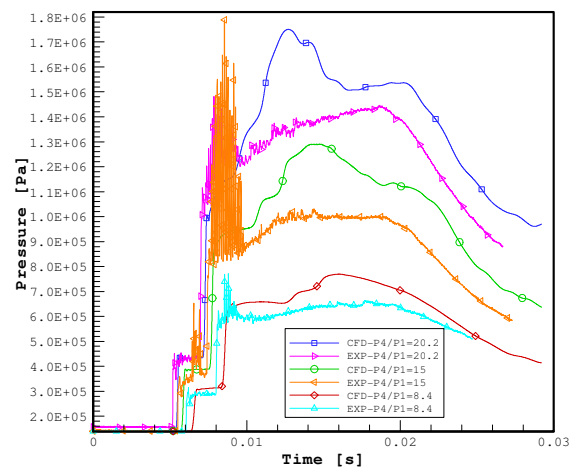

Figure 8: Pressure histories for different diaphragm pressure ratios (Air-Air experimental + CFD data)

As seen above, the CFD data can now be used with confidence after the validation has been made. In what follows, the pressure and temperature histories will be shown in Figures 9 and 10, respectively mainly to demonstrate the propagation of shock

wave within the barrel using CFD at pressure ratio=20. The results have been saved at every 0.005 second, showing clearly the reflection of shock wave from the right-end of the barrel. The highest temperature value of approximately 700K is observed at time level=0.015 second after the diaphragm rupture time. From the experimentation, the author has observed some water droplets near the diaphragm section. And this is due to the relatively low temperature value in the rarefaction region which is below the dew point temperature of the air. Interestingly enough, this phenomenon has been clearly demonstrated in the temperature contour plot as shown in Figure 10. However, from the depicted contour plots, it can be seen that the solution are wiggling. This may due to the unboundedness nature associated with the differencing scheme used in the current code.
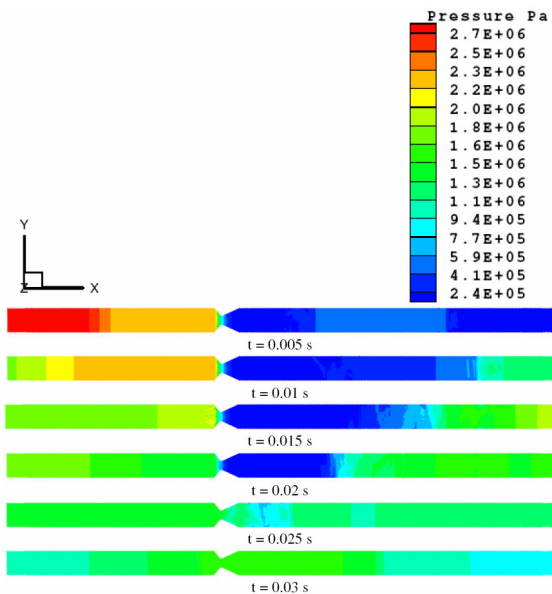
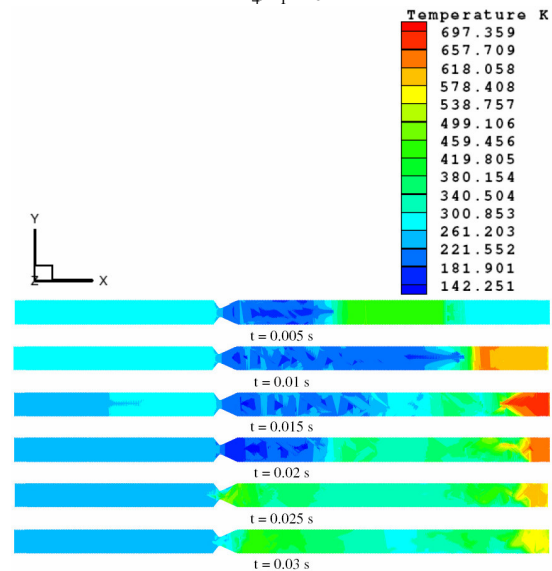Figure 9: Pressure Histories inside the shock tube, Air-Air $P_4/P_1=20$

Figure 10: Temperature Histories inside the shock tube, Air-Air $P_4/P_1=20$

Figure 11 shows the x-t diagram for different pressure ratios. As seen, the shock wave speed is increased when the pressure ratio is increased. The reflected shock wave coincides with contact surface which follows incident shock wave. Rarefaction wave, however, travels in the direction opposite the incident shock towards the driver section. Due to the existence of the bush, the

rarefaction wave is undergoing reflection within the driver section which is not desirable because it is sometimes useful to examine the flow condition at the region between the reflected rarefaction wave and the contact surface, which is more commonly known as the Region 3.

As shown in Figure 11, the maximum useful duration time can be obtained when the pressure ratio is prescribed as 20. The time is about 10 ms, which is quite comparable compared to other facilities.
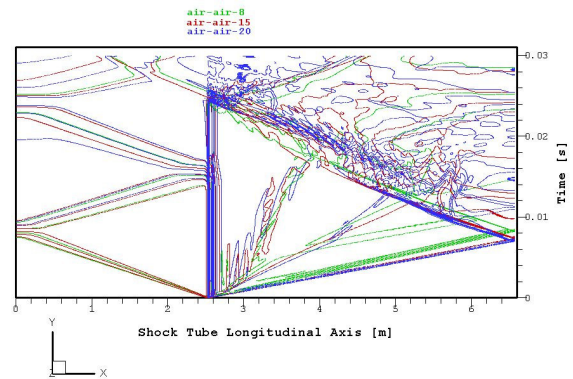

Figure 11: x-t diagram for three pressure ratios.

Figure 12 shows the surface temperature change of three different pressure ratios. It clearly shows that the difference in surface temperature increases as the pressure ratios increases and consequently enhance the heat loss to the surrounding (c.f. Figure 13), which is not preferable.
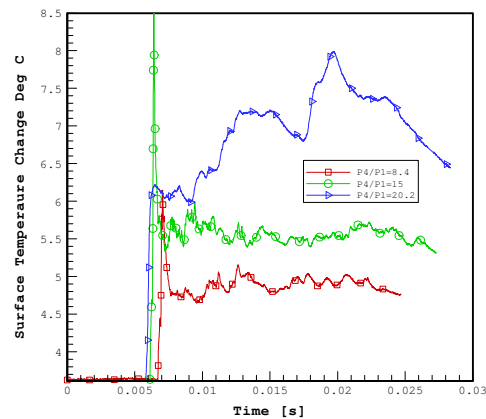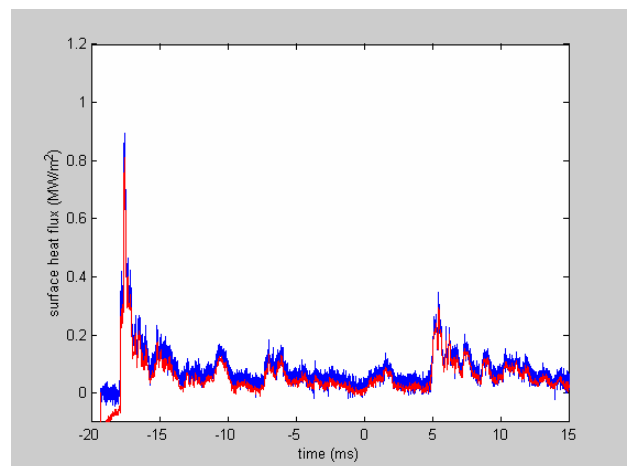

Figure 12: Surface temperature change profile

Figure 13: Heat flux profile

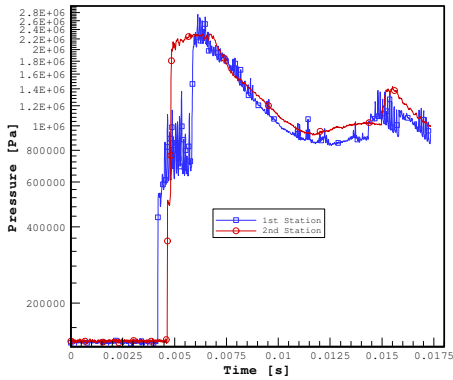## Experimentation for Dissimilar Gases

Figures 14 and 15 illustrate the pressure plots at the first and second stations for three different pressure ratios and different gas combination. Again, the shock strength improves when one enhances the pressure ratios. Similar trend goes for both the shock speed and the pressure peak.
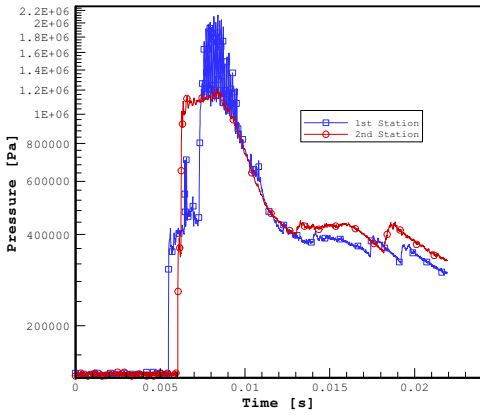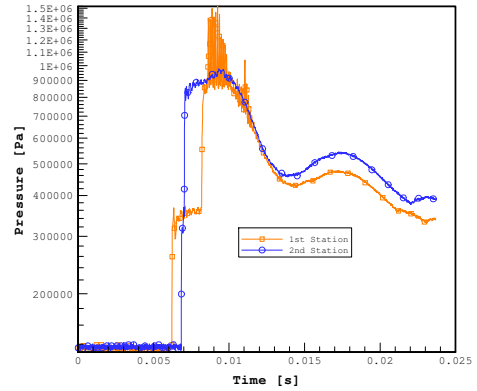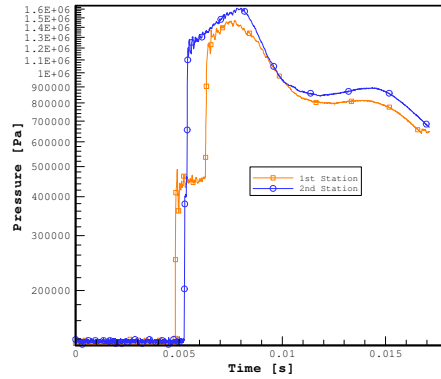

(a) $P_4/P_1=8.33$
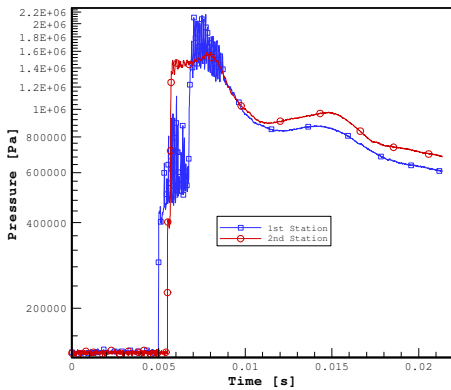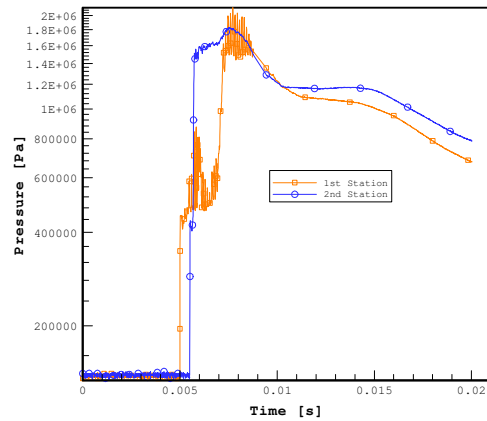

(b) $P_4/P_1=15$

(c) $P_4/P_1=20$

Figure 14: Experimental Pressure history inside the barrel for three different pressure ratios (He-Air)

(a) $P_4/P_1=8.4$

(b) $P_4/P_1=15$

(c) $P_4/P_1=20$

Figure 15: Experimental Pressure history inside the barrel (He-CO_2)

To summarise, Figure 16 compares the shock strength, shock speed and pressure peak for three different gas combinations at pressure ratio $P_4/P_1=20$. As seen, the He-Air combination produces the strongest shock wave, the greatest shock speed as well as the highest pressure peak, followed by the He-CO_2 and Air-Air combination.
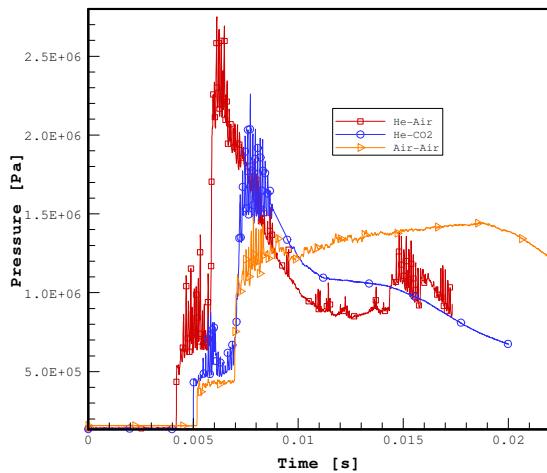
Figure 16: Shock wave generation for He-air, He-CO$_2$, and Air-Air

Figure 17 compares the surface temperature change for the gas combinations at pressure ratio P$_4$/P$_1$=20. As seen, the He-CO$_2$ combination produces the highest surface temperature change followed by the He-Air and Air-Air combination.
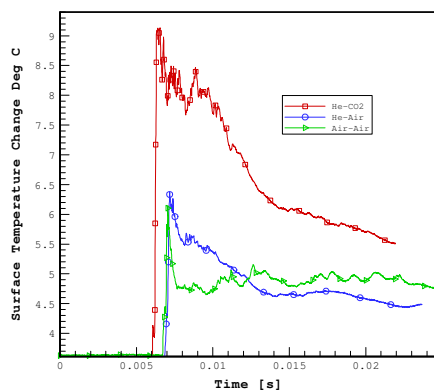

Figure 17: Surface Temperature Change at pressure ratio = 8.4

Shock Wave Velocity

The experimental shock wave velocities against the theoretical values are presented in Figure 18. The experimental results show that the shockwave velocity is fairly constant and somewhat less than theory predicts. This difference becomes larger as the diaphragm pressure ratio increases.
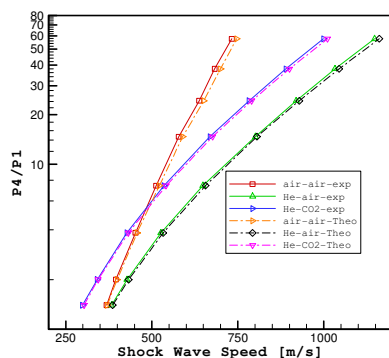

Figure 18: Shock wave speed

6.0 Conclusions

The results presented in this paper show that two-dimensional modeling of the hypersonic test facility is an effective way to obtain facility performance data. Although this paper focused on the HTF facility, the CFD code is generic and may be applied to other facilities.

The code could be further improved if a cylindrical coordinate system is used for mesh generation instead of the Cartesian coordinate system currently used. The experiments had successfully indicated the difference in simulation results when employing different working fluids combination. The results of the simulation showed a direct proportional relationship between Mach number and diaphragm pressure ratio and inverse proportion with speed of sound ratio.

Shock speed can be increased by raising the diaphragm pressure ratio, or more powerfully, by raising the speed of sound in the driver gas. To achieve high Mach numbers it is essential to raise the ratio of the speed of sound ratio (a_4/a_1) if excessive pressures are to be avoided. Shock speed now can be measured experimentally with the two pressure transducers technique easily.

Calculations showed that the combination of He-CO$_2$ is the best gas combination that can be used to get high Mach number. The tunnel will be operating on different operating conditions to produce strong shock wave for different applications. Higher Mach numbers can be achieved easily with relatively low diaphragm pressure ratios (i.e. to get Mach 6 we need to set P$_4$/P$_1$ to 465 if we use He/CO$_2$ and 192 if we use H$_2$/CO$_2$).

References

[1] Al-Falahi Amir, Zamri M , &Yusaf T (May-2007), "Numerical & Experimental Study to evaluate the effects of Diaphragm Pressure Ratio on Shock Wave strength and shock speed in a shock tube" Proceedings of the Third International Conference on Thermal Engineering: Theory and Applications May 21-23, 2007, Amman, Jordan

[2] Al-Falahi Amir, Yusaf T & Zamri M (2006) "Universiti Tenaga Nasional Short Duration Hypersonic Test Facility "Calibration and Verification" Proceeding of ESDA2006 8th Biennial ASME Conference on Engineering systems Design and Analysis July 4-7, 2006, Torino, Italy

[3] Al-Falahi Amir, Yusaf T & Yusoff M.Z "Hypersonic Free Piston Compression Wind Tunnel "Design & Construction" Proceeding of conference of Advances in Malaysian Energy Research 2004.© 2004 Malaysian Institute of Energy and Malaysia Energy Centre

[4] Zamri, M.Y. [1997] ' An improved treatment of two-dimensional Two-Phase Flow of Steam by a Runge Kutta Method', Ph.D. Thesis, University of Birmingham

[5] Gustafsson, B. and Sundstrom, A. [1978] *'Incompletely Parabolic Problem in Fluid Dynamics'* SIAM Journal of Applied Mathematics, 35 (2): 343-357

[6] Jameson, A., Schmidt, W. and Turkel, E. [1981] *'Numerical Solutions of the Euler Equations by Finite Volume Methods using Runge-Kutta Time Stepping Schemes'* AIAA Paper No. 81-1259

[7] Swanson, R.C. and Radespiel, R. [1991] *'Cell Centred and Cell Vertex Multigrid Schemes for the Navier Stokes Equations.'* AIAA Journal May 1991

[8] D.R. Buttsworth, P.A. Jacobs, and T.V. Jones, "Simulation of Oxford University Gun Tunnel performance using a quasi-0ne-dimensional model", Shock Waves (2002) 11: 377–383

[9] Mohd. Zamri Yusoff, "A Two-Dimensional Time-Accurate Euler Solver for Turbo machinery Applications" Journal-Institution of Engineers, Malaysia Vol. 5 No. 3 1998

[10] D.R. Buttsworth, "Heat transfer during transient compression: measurements and simulation", Shock Waves (2002) 12:87-91.

[11] Jhon D. Anderson, Modern Compressible Flow with Historical Perspective, McGraw Hill, New York, 1990.

[12] P.A. THOMPSON (1972), Compressible Fluid Dynamics, McGraw Hill.

[13] P.A. Jacobs, "Quasi-One-Dimensional Modeling of a Free-Piston Shock Tunnel" AIAA Jornal, Vol.32, No. 1, Januray 1994.

[14] Alan Pope & Kennith L. Goin, High-Speed Wind Tunnel Testing, John Wiely, New York 1965.

[15] East, R.A., "The performance and operation of the University of Southampton hypersonic gun tunnel," Univ. of Southampton Aero. and Astro. Rep. no. 135, I960.

[16] H. GRÖNIG (1987), Shock Tubes and Waves, *Proceedings of the 16th International Symposium on Shock Tubes and Waves*, Aachen, Germany, July 26-31, VCH Publishers.

[17] K. N. C. Bray, Evaluation of The Hypersonic Gun Tunnel, Proceedings of the ARS International Hypersonic Conference, August, 1961.

[18] D.R. Buttsworth and Peter A. Jacobs, "Total Temperature Measurments in a shock Tunnel Facility", 13th Australian Fluid Mechanics Conference, Monash university, Melbourne, Australia, 1998

[19] Cooley, J.W. & Tukey, J.W., An Algorithm for the Machine Computation of Complex Fourier Series, *Math. Comp.*,**19**, 1965, 297-301.

[20] Goosens, M., Mittlebach, F. & Samarin, A., *The LaTeX Companion*, Addison-Wesley, 1994.

[21] McCormick, S., Multilevel Projection Methodology, in *Computational Techniques and Applications: CTAC93*, editors D. Stewart, H. Gardner and D. Singleton, World Scientific, 1994, 54-57.

[22] Rosenhead, L. (editor) *Laminar Boundary Layers* Oxford, Clarendon Press, 1963.